Chapter 4
REVIEW OF PROPOSED CONSTITUTIVE MODELS FOR CHALK

As shown in chapter 3, chalk is characterized by nonlinear stress-strain behavior, time-dependent deformations, and pore fluid-dependent behavior. Formulation of a single constitutive model that describes these aspects of chalk behavior is challenging. This chapter contains a review of the individual constitutive models that have been proposed to describe the various aspects of chalk behavior.

The discussion on constitutive models for chalk is separated into three topics: elastoplastic and elastoviscoplastic models, time-dependent models only, and rock-fluid interaction models only. Several of the proposed models are included in more than one category. Due to their relative simplicity, nonlinear elastic models have been used to simulate the behavior of chalk (Potts et al., 1988; Chin et al., 1993). The nonlinear elastic models which have been applied to chalk will not be reviewed here. Only models formulated in the framework of elasto(visco)plasticity are included here.

ELASTO(VISCO)PLASTIC MODELS

A summary of the elastic and elastoviscoplastic models that have been proposed for chalk is included in Table 4.1.

Table 4.1. Summary of Elasto(visco)plastic Constitutive Models for Chalk

Model # 1	Reference	DeGennaro et al. (2003), Collin et al. (2002), Datcheva et al. (2001), PASACHALK (2004)
	Number of independent yield mechanisms	3
	Description of yield surfaces in 2 dimensions (*p*-*q* space)	1. Pore collapse: elliptical yield surface with associated plastic flow and isotropic hardening 2. Shear: straight-line yield surface with non-associated plastic flow and isotropic hardening 3. Tensile failure: vertical straight-line yield surface with associated plastic flow, no hardening
	3-dimensional effects	Van Eekelen (1980) surface in π-plane
	Elasticity	Option for linear or nonlinear elasticity
	Time-dependent deformations	None included in Collin et al.; overstress viscoplasticity included in DeGennaro et al., Datcheva et al., PASACHALK
	Effect of saturating fluid	Uses Barcelona Basic Model (BBM) (Alonso et al., 1990): Size of shear and pore collapse yield surfaces change depending on suction, which is defined as the difference between oil pressure and water pressure. Note that Datcheva et al. do not account for pore fluid dependence.

Table 4.1 (continued). Summary of Elasto(visco)plastic Constitutive Models for Chalk

Model # 2	Reference	Homand and Shao (2000); follows from Homand et al. (1998) and Schroeder and Shao (1996)
	Number of independent yield mechanisms	2
	Description of yield surfaces in 2 dimensions (*p*-*q* space)	1. Pore collapse: elliptical yield surface with non-associated plastic flow and isotropic hardening 2. Shear: straight-line yield surface with non-associated plastic flow and isotropic hardening
	3-dimensional effects	Mohr-Coulomb surface in π-plane
	Elasticity	Linear elasticity
	Time-dependent deformations	None
	Effect of saturating fluid	Two yield surfaces with different initial sizes exist; one is for "oil-like" saturating fluid, one is for "water-like" saturating fluid
Model # 3	Reference	Gutierrez (1998, 1999, 2000)
	Number of independent yield mechanisms	3
	Description of yield surfaces in 2 dimensions (*p*-*q* space)	1. Pore collapse: elliptical cap yield surface with associated plastic flow and isotropic hardening 2. Shear: straight-line yield surface with non-associated plastic flow, smooth transition to pore collapse surface, no hardening 3. Tensile failure: curved yield surface with associated plastic flow, no hardening
	3-dimensional effects	William-Warnke (1975) surface in π-plane
	Elasticity	Linear elasticity
	Time-dependent deformations	Rate-type model based on volumetric creep model of Bjerrum (1967)
	Effect of saturating fluid	Creep parameter varies as a function of saturating fluid; change in pore fluid is seen as a modification of time-dependent behavior
Model # 4	Reference	Papamichos et al. (1997)
	Number of independent yield mechanisms	1
	Description of yield surfaces in 2 dimensions (*p*-*q* space)	Modified surface includes effects of pore collapse and shearing: modified straight-line yield surface at low mean stress transitions to cap-like yield surface at high mean stress, with non-associated plastic flow and isotropic hardening; both friction angle and preconsolidation stress are hardening parameters
	3-dimensional effects	Mohr-Coulomb surface in π-plane
	Elasticity	Linear elasticity
	Time-dependent deformations	None
	Effect of saturating fluid	Size of initial yield surface depends on water saturation

Table 4.1 (continued). Summary of Elasto(visco)plastic Constitutive Models for Chalk

Model # 5	Reference	Plischke (1994, 1996)
	Number of independent yield mechanisms	2
	Description of yield surfaces in 2 dimensions (*p*-*q* space)	1. Pore collapse: elliptical yield surface with associated plastic flow and isotropic hardening 2. Shear: straight-line yield surface with non-associated plastic flow, no hardening
	3-dimensional effects	None
	Elasticity	Linear elasticity
	Time-dependent deformations	Only related to water injection
	Effect of saturating fluid	Size of initial yield surface depends on water saturation
Model # 6	Reference	Foged et al. (1995)
	Number of independent yield mechanisms	2, with transition surface joining them
	Description of yield surfaces in 2 dimensions (*p*-*q* space)	1. Pore collapse: elliptical yield surface with associated plastic flow and isotropic hardening 2. Shear: straight-line yield surface with non-associated plastic flow, no hardening
	3-dimensional effects	Drucker-Prager surface in π-plane
	Elasticity	Not specified
	Time-dependent deformations	None
	Effect of saturating fluid	None
Model # 7	Reference	Abdulraheem et al. (1993)
	Number of independent yield mechanisms	2
	Description of yield surfaces in 2 dimensions (*p*-*q* space)	1. Pore collapse: elliptical yield surface with associated plastic flow and isotropic hardening 2. Shear: straight-line yield surface with non-associated plastic flow, no hardening
	3-dimensional effects	None
	Elasticity	Not specified
	Time-dependent deformations	None
	Effect of saturating fluid	None

Table 4.1 (continued). Summary of Elasto(visco)plastic Constitutive Models for Chalk

Model # 8	Reference	Shao and Henry (1991)
	Number of independent yield mechanisms	2
	Description of yield surfaces in 2 dimensions (*p*-*q* space)	1. Pore collapse: p = constant straight-line yield surface with associated plastic flow and isotropic hardening 2. Shear: modified straight-line yield surface (Lade, 1984) with non-associated plastic flow and isotropic hardening
	3-dimensional effects	Lade (1984) surface in π-plane
	Elasticity	Nonlinear elasticity
	Time-dependent deformations	None
	Effect of saturating fluid	None

The various yield surfaces and constitutive equations for the proposed chalk models are shown in Figures 4.1 to 4.8.

The eight elasto(visco)plastic models described in Table 4.1 have many similarities with a few key differences:

- Seven of the eight constitutive models (*i.e.*, all except that of Papamichos et al. (1997)) are multi-mechanism models which have separate yield surfaces for the shearing and pore collapse yield mechanisms;
- All models are formulated with enclosed yield surfaces that show the effects of yielding and/or failure due to pore collapse and shearing, while some also include yield surfaces for tensile failure;
- All models except the model of Shao and Henry (1991) model the pore collapse yield surface as an elliptical or near-elliptical cap surface;
- Most models, including all except that of Papamichos et al. (1997), model the shear and pore collapse yield surfaces independently such that evolution of one yield surface does not modify the other;
- All models include non-associated plasticity for the shear yield surface;
- Most models include associated plasticity for the pore collapse yield surface; only the single-surface model of Papamichos et al. (1997) and the model of Homand and Shao (2000) specify non-associated plasticity for the pore collapse mechanism;
- All models are characterized by isotropic hardening for the hardening yield surfaces;
- All models include hardening to the pore collapse yield surface; and,

- Most models, including the two most recently proposed, include hardening to the shear yield surface.

From the review of constitutive models for chalk, it may be concluded that only minor differences exist regarding the description of time-independent elastoplastic behavior of chalk. Less agreement between models exists regarding the best description of time-dependent behavior and effect of saturating fluid on mechanical behavior.

TIME-DEPENDENT MODELS

The various time-dependent models that have been proposed to simulate chalk behavior are described in the following paragraphs.

The constitutive models of DeGennaro et al. (2003), Datcheva et al. (2001), and Gutierrez (1999, 2000) have provisions for time-dependent behavior. Of these, the models of DeGennaro et al. and Datcheva et al. are overstress elastoviscoplasticity models. Viscoplastic strain rate varies exponentially with overstress in these models. The reference surface for these time-dependent models is not the yield surface but is smaller and has a similar shape as the yield surface (Figure 4.9). Therefore, irreversible strains occur even at stress states below the yield surface. Overstress elastoviscoplasticity models are described by a function for the reference surface, at least one viscosity parameter, and a function between yield function f and viscoplastic strain magnitude Φ.

The Unified Chalk Model (UCM) of Gutierrez (1999, 2000) is formulated as a rate-type model. The UCM uses the logarithmic model of Bjerrum (1967). In this case, the viscoplastic volumetric strain rate is inversely proportional to the volumetric age of the material. The volumetric age is proportional to the distance in stress space between the stress point and the pore collapse yield surface (Figure 4.10). All viscoplastic strain components are scaled from the viscoplastic volumetric strain; viscoplastic strains occur only for stress states that may be mapped onto the pore collapse yield surface. Borja and Kavazanjian (1985) applied a similar model to the Modified Cam-Clay model using both the volumetric scaling used by Gutierrez and a deviatoric scaling option. Rate-type models are described by a function for material age and a creep parameter.

In addition to these constitutive models, the creep behavior of chalk has been modeled by Andersen et al. (1992) using the logarithmic rate-type model of deWaal (1986) which was developed for soft reservoir rocks. This model is very similar to that of Bjerrum but is formulated using lines on which stress rate is equal (Figure 4.11) rather than time-lines on which age and viscoplastic strain rate are equal. Use of deWaal's model produces the same behavior as Bjerrum's model, but this model makes no reference to material age.

Another approach to simulating creep in chalk was proposed by Rhett (1994) using a linear relation between (1/time) and (1/strain). This type of model produces a hyperbolic relation between creep duration and creep strain (Figure 4.12).

The differences between the various time-dependent models described above are summarized as follows:

- Overstress elastoviscoplasticity models and rate-type models are based on the relative positions of the stress point and reference or yield surface in stress space. Therefore, time-dependent behavior does not depend on loading history, which is consistent with laboratory test results;
- The hyperbolic model does not differentiate between time-dependent and time-independent irreversible strains. Therefore, time-dependent behavior must depend on loading history; and,
- Overstress elastoviscoplasticity models and rate-type models have no limiting strain value, which makes them physically unrealistic in the limit as creep continues. Hyperbolic models are characterized by a limiting value.

PORE FLUID-DEPENDENT MODELS

As related to effects of saturating fluid, several different models have been proposed to describe this behavior. The various models are described in the following paragraphs.

The pore fluid-dependent model of DeGennaro et al. (2003) and Collin et al. (2002) is the Barcelona Basic Model (BBM) proposed by Alonso et al. (1990) for unsaturated soils. The BBM is formulated using suction, which is equal to the difference between oil and water pressures in chalk, as an independent variable. The BBM separates irreversible strains into mechanical and suction-based components. The model of DeGennaro et al. and Collin et al. is formulated such that that both cohesion and preconsolidation stress vary with suction, but friction angle is

independent of suction. The basic elements of the BBM as applied to chalk are illustrated in Figure 4.13.

The pore fluid-dependent model of Homand and Shao (2000) is formulated so that irreversible strains are generated if the water saturation increases from a value less than the critical value to a value greater than the critical value. In contrast to the BBM, the variation in yield surface not continuous but instead is abrupt, occurs at some critical value of water saturation, and does not depend on suction. The yield surfaces contract when water saturation increases to a critical value. If the force on a sample remains constant during a decrease in suction, large irreversible strains are produced. In the model of Homand and Shao, the cohesion, friction angle, and preconsolidation stress all change when water saturation increases to the critical value (Figure 4.14).

Gutierrez (1999, 2000) formulates the pore fluid-dependent model only as a modification to time-dependent behavior. This model is formulated so that the creep parameter ψ increases as water saturation increases. Since the age of the chalk depends on the creep parameter in the time-dependent model of Gutierrez, the viscoplastic strain rate increases when ψ increases, even though the yield surface undergoes no instantaneous change. Only the pore collapse yield mechanism is a function of the pore fluid-dependent model; the shear yield behavior is not affected by pore fluid composition in this model.

Pore fluid dependence is included in the model of Papamichos et al. (1997) in much the same way as for the models of DeGennaro et al. and Collin et al. Both the tension cut-off (which acts as a surrogate for cohesion) and preconsolidation stress vary as a function of water saturation. While the weakening mechanism is attributed to changes in capillary forces, the model is not formulated in terms of suction. The elastic modulus also decreases as water saturation increases, while Poisson's ratio is not affected.

The pore fluid-dependent model of Piau et al. (1998), Maury et al. (1996), and Piau and Maury (1994, 1995) is formulated using the concept of the "yield surface jump at the waterfront" (YSJW). This concept is much like the model of Papamichos et al. in that the yield surface changes continuously as a function of water saturation. Both the shear yield surface and pore collapse surface are affected by water saturation in this formulation. The friction angle, critical shear stress ratio, and preconsolidation stress all change with water saturation (Figure 4.15).

Plischke (1994, 1996) includes a pore fluid-dependent component in simulating the effects of waterflooding. In this model, the preconsolidation stress decreases gradually as water saturation increases. An explicit function which relates water saturation to preconsolidation stress is not given.

The majority of models vary the size of the initial yield surface as a function of the water saturation or of the suction, such that changing the pore fluid causes an instantaneous change in the position of the yield surface. The UCM of Gutierrez considers the effects of saturating fluid in a different way, as a parameter on which creep parameter depends.

REFERENCES

Abdulraheem, A., Zaman, M., and Roegiers, J.C. (1993). Numerical simulation of a compacting reservoir. International Journal of Rock Mechanics and Mining Sciences and Geomechanics Abstracts, 30 (7), 1299-1302.

Alonso, E.E., Gens, A., and Josa, A. (1990). A constitutive model for partially saturated soils. Geotechnique, 40(3), 405-430.

Andersen, M.A., Foged, N., and Pedersen, H.F. (1992). The link between waterflood-induced compaction and rate-sensitive behaviour in weak North Sea chalk. Proceedings of the 4th North Sea Chalk Symposium, Deauville, France, 15 p.

Bjerrum, L. (1967). Engineering geology of Norwegian normally consolidated marine clays as related to settlements of buildings. 7th Rankine Lecture, Geotechnique, 17 (2), 83-117.

Borja, R.I. and Kavazanjian, E. (1985). A constitutive model for the stress-strain-time behavior of wet clays. Geotechnique, 35 (3), 283-298.

Chin, L, Boade, R.R., Prevost, J.H., Landa, G.H. (1993). Numerical simulation of shear-induced compaction in the Ekofisk reservoir. International Journal of Rock Mechanics and Mining Sciences and Geomechanics Abstracts, 30(7), 1193-1200.

Collin, F., Cui, Y.J., Schroeder, C., and Charlier, R. (2002). Mechanical behavior of Lixhe chalk partly saturated by oil and water: experiment and modeling. International Journal for Numerical and Analytical Methods in Geomechanics, 26, 897-924.

Datcheva, M., Charlier, R., and Collin, F. (2001). Constitutive equations and numerical modeling of time effects in soft porous rocks. Lecture Notes in Computer Science, 1988, 222-229.

DeGennaro, V., Delage, P., Cui, Y.-J., Schroeder, C., and Collin, F. (2003). Time-dependent behaviour of oil reservoir chalk: a multiphase approach. Soils and Foundations, 43(4), 131-147.

deWaal, J.A. (1986). On the Rate-Type Compaction Behavior of Sandstone Reservoir Chalk. Ph.D. thesis, Delft Univ. of Technology, The Netherlands.

Foged, N., Krogsboll, A., Hansen, C.F., Jorgensen, K.Z., Christensen, H.F., and Jepsen, J.E. (1995). Modeling of stresses and fractures in a reservoir, EFP-93 Final Report to DEA.

Gutierrez, M.S. (1998). Formulation of a Basic Chalk Constitutive Model, NGI Report no. 541105-2.

Gutierrez, M.S. (1999). Modelling of Time-Dependent Chalk Behavior and Chalk-Water Interaction, NGI Report no. 541105-4.

Gutierrez, M.S. (2000). Formulation of a 3-D stress-strain-time model for chalk. Contract report to Phillips Petroleum Company.

Homand, S., and Shao, J.F. (2000). Mechanical behavior of a porous chalk and effect of saturating fluid. Mechanics of Cohesive-Frictional Materials, 5, 583-606.

Homand, S., Shao, J.F., and Schroeder, C. (1998). Plastic modeling of compressible porous chalk and effect of water injection. Proceedings of EUROCK '98, Trondheim, Norway, 495-504.

Lade, P.V. (1984). Modelling rock strength in three dimensions. International Journal of Rock Mechanics and Mining Sciences and Geomechanics Abstracts, 21, 21-33.

Maury, V. , and Piau, J-.M. (1996). Subsidence induced by water injection in water-sensitive reservoir rocks: The example of central Ekofisk. Proceedings of the 5th North Sea Chalk Symposium, Reims, France, 23 p.

Papamichos, E., Brignoli, M., and Santarelli, F.J. (1997). An experimental and theoretical study of a partially saturated collapsible rock. Mechanics of Cohesive-Frictional Materials, 2, 251-278.

PASACHALK (2004). Mechanical Behavior of Partially and Multiphase Saturated Chalks Fluid-Skeleton Interaction: Main Factor of Chalk Oil Reservoirs Compaction and Related Subsidence – Part 2, Final Report, EC Contract no. ENK6-2000-00089.

Piau, J-.M., Bois, A.-P., Atahan, C., and Maury, V. (1998). Water/chalk (or collapsible soil) interaction: Part I. Comprehensive evaluation of strain and stress jumps at the waterfront. Proceedings of EUROCK '98, Trondheim, Norway, 419-427.

Piau, J-.M. and Maury, V. (1995). Basic mechanical modelisation of chalk/water interaction. Proceedings of the First International Conference on Unsaturated Soils, Paris, 8 p.

Piau, J-.M. and Maury, V. (1994). Mechanical effects of water injection on chalk reservoirs. Proceedings of EUROCK '94, Delft, The Netherlands, 819-827.

Plischke, B. (1994). Finite element analysis of compaction and subsidence - Experience gained from several chalk fields. Proceedings of EUROCK '94, Delft, The Netherlands, 795-802.

Plischke, B. (1996). Some aspects of numerical simulation of water-induced chalk compaction. Proceedings of the 5th North Sea Chalk Symposium, Reims, France, 13 p.

Potts, D.M., Jones, M.E., and Berget, O.P. (1988). Subsidence above the Ekofisk oil reservoirs. Proceedings of BOSS '88, 113-127.

Rhett, D.W. (1994). The mechanics of time-dependent strain in high-porosity North Sea chalk. Proceedings of the EAPG/AAPG Special Conference on Chalk, Copenhagen, Denmark.

Schroeder, C. and Shao, J.F. (1996). Plastic deformation and capillary effects in chalks. Proceedings of the 5th North Sea Chalk Symposium, Reims, France, 14 p.

Shao, J.F. and Henry, J.P. (1991). Development of an elastoplastic model for porous rock. International Journal of Plasticity, 7, 1-13.

Van Eekelen, H.A.M. (1980). Isotropic yield surfaces in three dimensions for use in soil mechanics. International Journal for Numerical and Analytical Methods in Geomechanics, 4, 98-101.

William, K.J. and Warnke, E.P. (1975). Constitutive model for the triaxial behavior of concrete, ISMES Seminar on Concrete Structures Subjected to Triaxial Stress, Bergamo, Italy, 1-30.

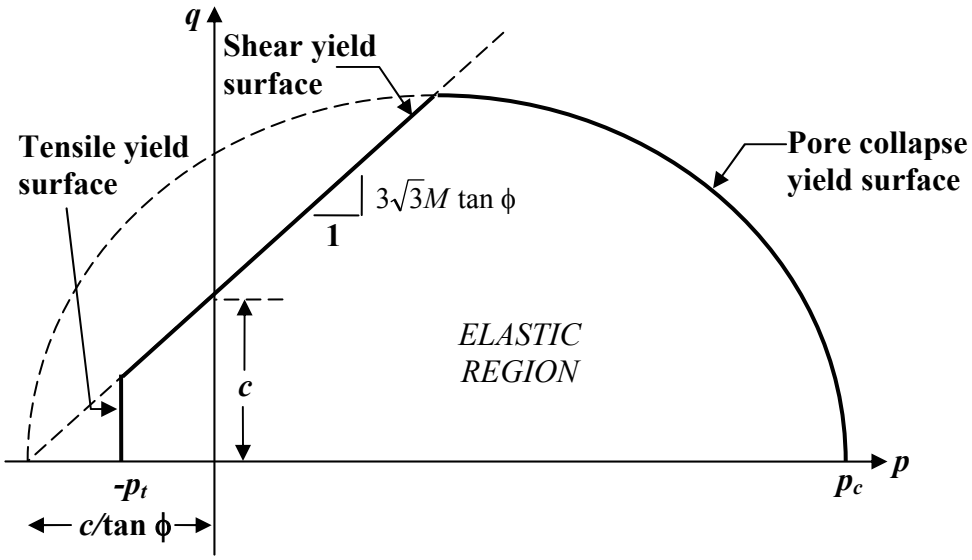

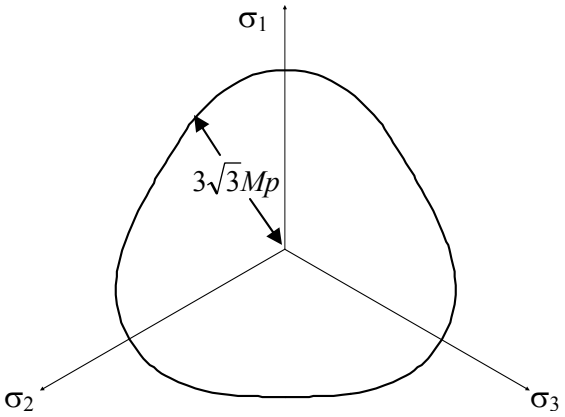

$$f_c = q^2 + 27M^2\left(p + \frac{c}{\tan\phi}\right)(p - p_c) \qquad g_c = f_c$$

$$f_s = q - 3\sqrt{3}M\left(p + \frac{c}{\tan\phi}\right) \qquad g_s = q - 3\sqrt{3}M'\left(p + \frac{c}{\tan\phi}\right)$$

$$f_t = p - p_t \qquad g_t = p - p_t$$

$$M = a(1 + b\sin 3\theta)^n \qquad M' = a'(1 + b\sin 3\theta)^n$$

$$p_c = p_{c0}\exp\left(\frac{1+e}{\lambda - \kappa}\varepsilon_v^p\right)$$

$$\phi = \phi_0 + (\phi_p - \phi_0)\frac{\varepsilon_s^p}{B + \varepsilon_s^p}$$

$$c = c_0 + (c_p - c_0)\frac{\varepsilon_s^p}{B + \varepsilon_s^p}$$

ϕ	friction angle
c	cohesion
p_c	preconsolidation stress
p_t	tensile strength
λ	compression coefficient
κ	recompression coefficient
a,b,n,B	fitting parameters

Figure 4.1. Elastoplastic model of DeGennaro et al. (2003), Collin et al. (2002), Datcheva et al. (2001), shown in the meridian plane and in the π-plane (Van Eekelen surface).

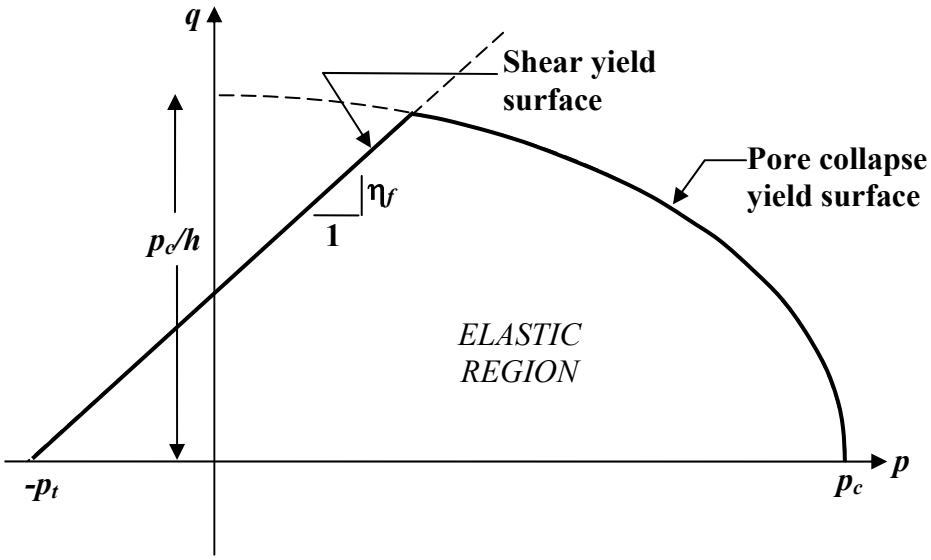

$$f_c = h^2 q^2 + p^2 - p_c^2$$
$$g_c = h_c^2 q^2 + p^2$$
$$f_s = q - \eta_f (p + p_t)$$
$$g_s = q - p\eta_g$$
$$p_c = p_{c0} \exp\left(a\varepsilon_v^p\right)$$
$$\eta_f = \eta_p - (\eta_p - \eta_0)\exp\left(-b\varepsilon_s^p\right)$$
$$\eta_g = \eta_{g0} \exp\left(-b\varepsilon_s^p\right)$$

η_f	yield shear stress ratio
η_g	dilatancy ratio
$\eta_0, \eta_{g0}, \eta_p$	initial and peak ratios
h, h_c	aspect ratio of ellipses
p_c	preconsolidation stress
p_t	tensile strength
a, b	fitting parameters

Figure 4.2. Elastoplastic model of Homand and Shao (2000), shown in the meridian plane.

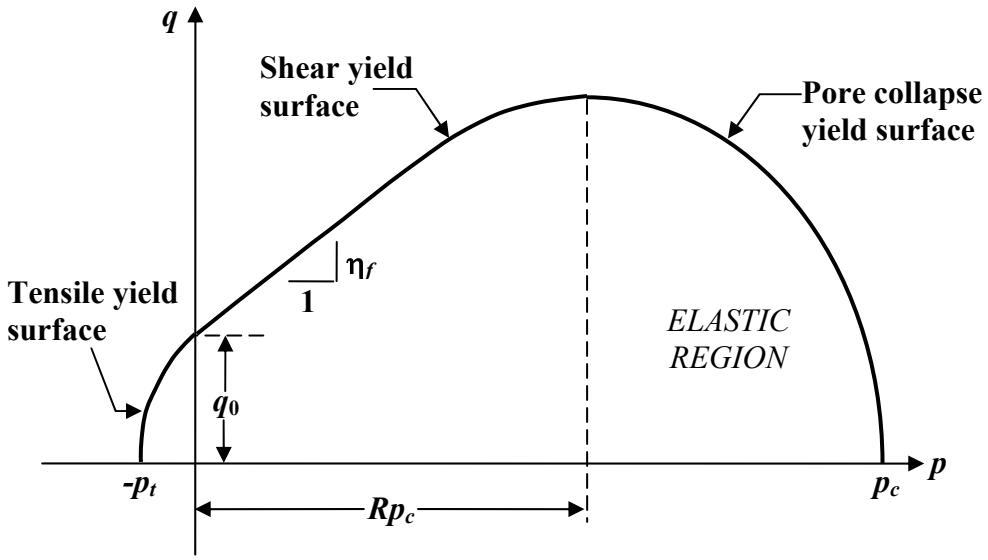

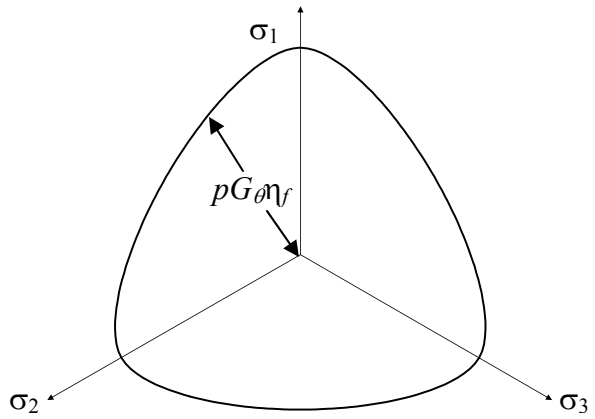

$$f_c = q^2 - \left(q_0 + \sqrt{\alpha^2 + \left(\eta_f R p_c\right)^2} - \alpha \right)^2 \left[1 - \left(\frac{p - R p_c}{p_c (R-1)} \right)^2 \right]$$

$$g_c = f_c$$

$$f_s = q - q_0 - \sqrt{\alpha^2 + \left(\eta_f R p_c\right)^2} + \sqrt{\alpha^2 + \left[\eta_f \left(p - R p_c\right)\right]^2}$$

$$g_s = q + \sqrt{\alpha^2 + \left[\eta_g \left(p - R p_c\right)\right]^2}$$

$$f_t = q^2 - q_0 \left[2p \frac{\eta_f^2 R p_c}{\sqrt{\alpha^2 + \left(\eta_f R p_c\right)^2}} \left(1 + \frac{p}{p_t} \right) + q_0 \left(1 - \frac{p^2}{p_t^2} \right) \right]$$

$$g_t = f_t$$

$$p_c = p_{c0} \exp\left(\frac{1+e}{\lambda - \kappa} \varepsilon_v^p \right)$$

η_f	yield shear stress ratio
η_g	dilatancy ratio
p_c	preconsolidation stress
p_t	tensile strength
α	curvature of shear surface
q_0	cohesion parameter
λ	compression coefficient
κ	recompression coefficient
R	ellipse size parameter

Figure 4.3. Elastoplastic model of Gutierrez (1998, 2000), shown in the meridian plane and in the π-plane (William-Warnke surface).

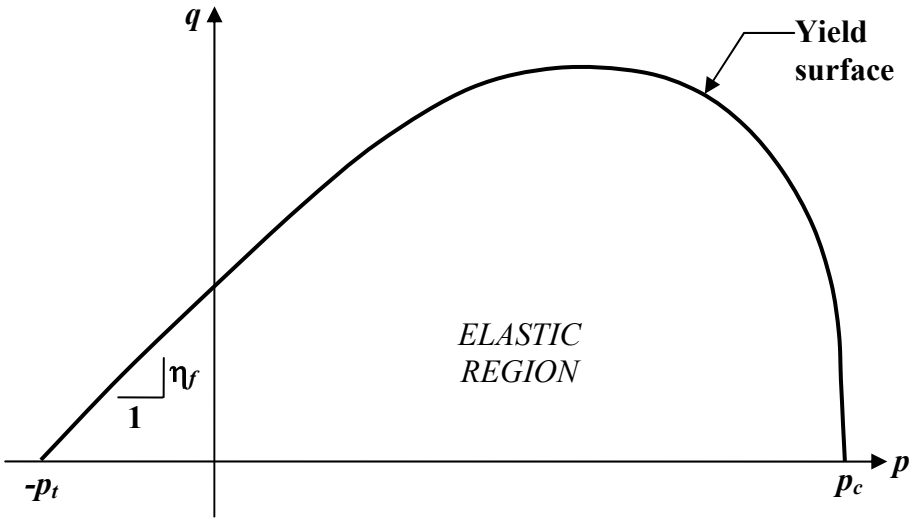

$$f = q - \eta_f (p + p_t)\sqrt{\frac{p_c - p}{p_t + p_c}}$$

$$g = q - \eta_g (p + p_t)\sqrt{\frac{p_c - p}{p_t + p_c}}$$

$$p_c = p_{c0} \exp\left(b\varepsilon_v^p\right)$$

$$\eta_f = \eta_p - (\eta_p - \eta_0)\exp\left(-b\varepsilon_s^p\right)$$

η_f	yield shear stress ratio
η_g	dilatancy ratio
η_0 ,η_p	initial and peak ratios
p_c	preconsolidation stress
p_t	tensile strength
b	fitting parameters

Figure 4.4. Elastoplastic model of Papamichos et al. (1997), shown in the meridian plane.

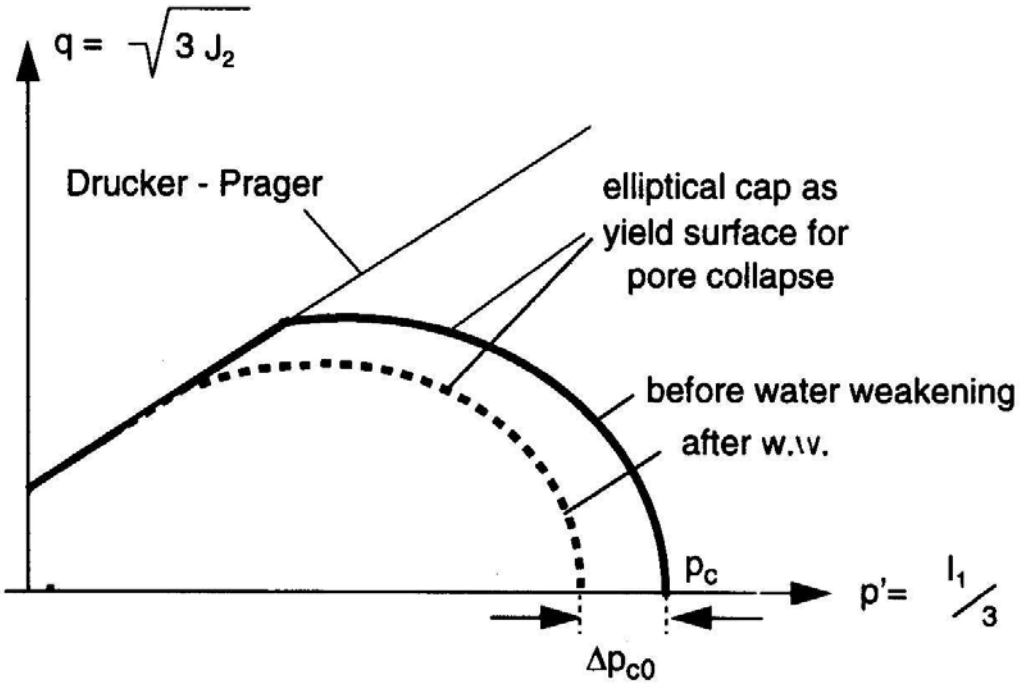

Figure 4.5. Elastoplastic model of Plischke (1994, 1996) shown in the meridian plane (Plischke, 1996).

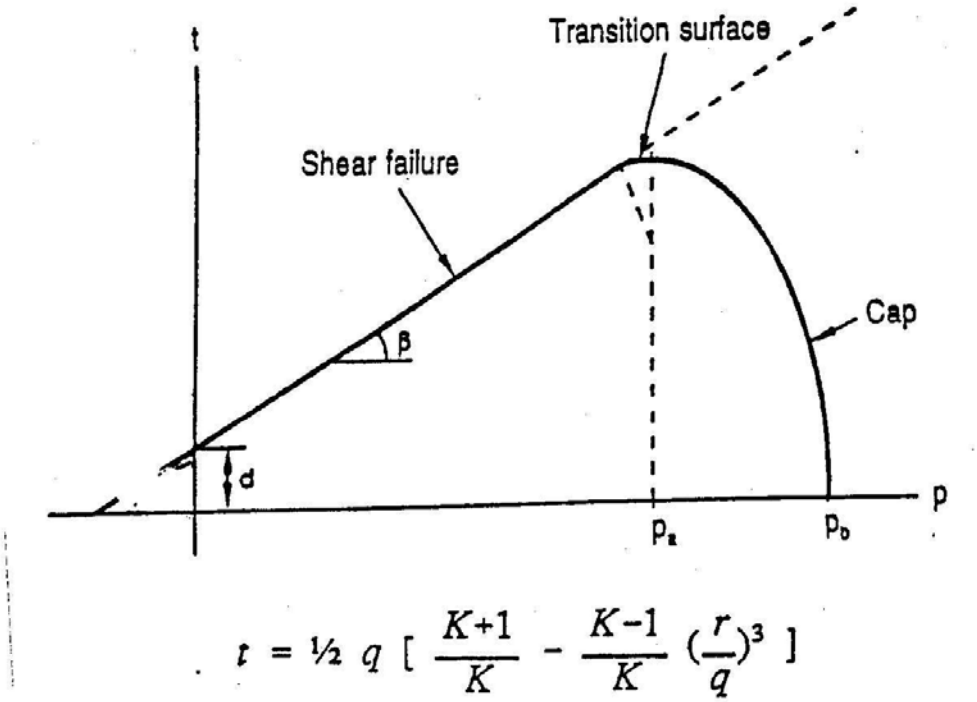

Figure 4.6. Elastoplastic model of Foged et al. (1995) shown in the meridian plane (Foged et al., 1995).

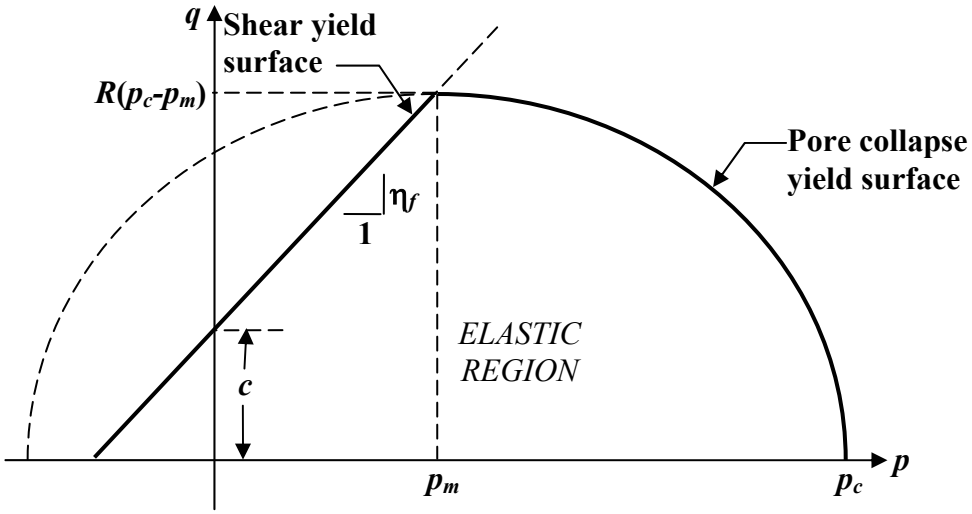

$$f_c = q - \sqrt{R^2 (p_c - p_m) - (p - p_m)}$$
$$g_c = f_c$$
$$f_s = q - \eta_f p - c$$
$$g_s = f_s$$
$$p_c = p_{c0} + a\left(\varepsilon_{ij}^p \varepsilon_{ij}^p\right)^n$$

η_f	yield shear stress ratio
c	cohesion
p_c	preconsolidation stress
p_m	center of ellipse
R	aspect ratio for ellipse
a,n	fitting parameters

Figure 4.7. Elastoplastic model of Abdulraheem et al. (1993) shown in the meridian plane.

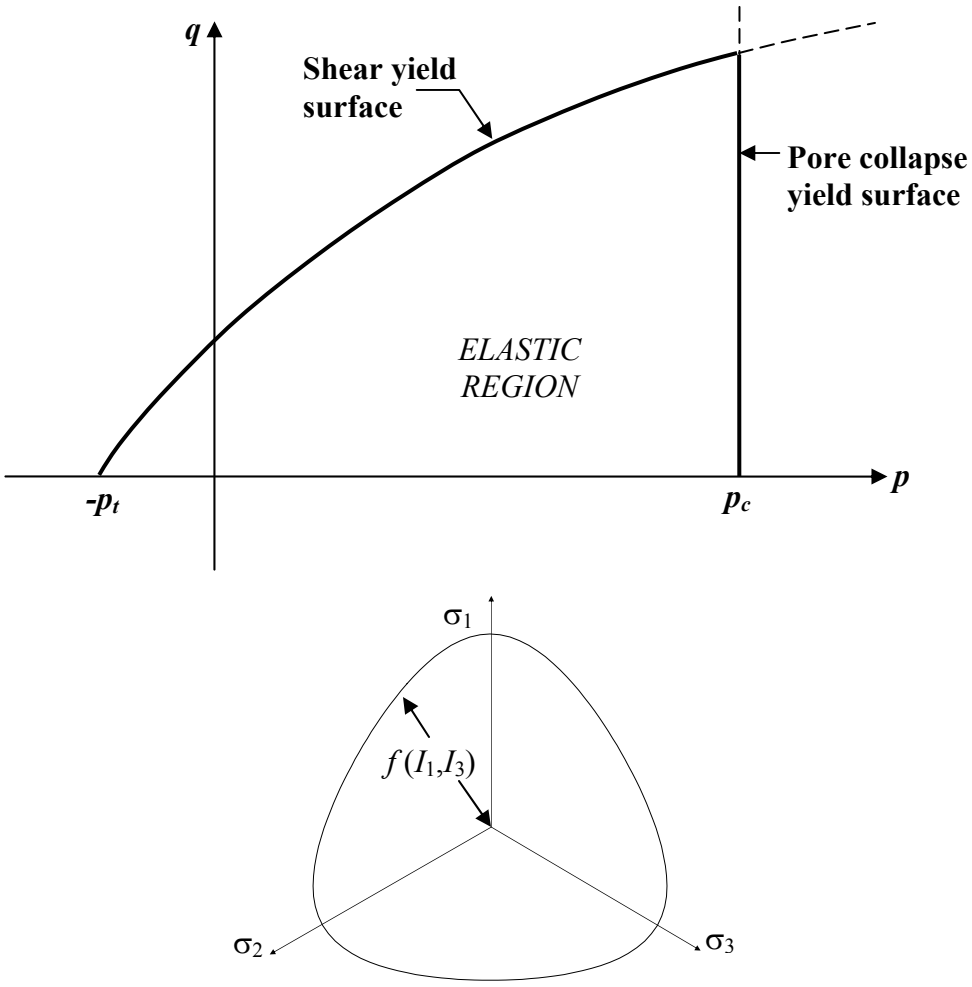

$$f_c = p - p_c$$

$$f_c = g_c$$

$$f_s = \left(\frac{\bar{I}_1^3}{\bar{I}_3} - 27 \right) \left(\frac{\bar{I}_1}{p_a} \right)^n - m$$

$$g_s = \bar{I}_1^3 - 27\bar{I}_3$$

$$\bar{I}_1 = 3(p + p_t)$$

$$\bar{I}_3 = (\sigma_1 + p_t)(\sigma_2 + p_t)(\sigma_3 + p_t)$$

$$p_c = p_{c0} + a p_a \varepsilon_v^p \exp(b\varepsilon_v^p)$$

$$m = m_0 \frac{\varepsilon_s^p}{c + d\varepsilon_s^p}$$

c	cohesion
p_c	preconsolidation stress
p_a	atmospheric pressure
p_t	tensile strength
m	Lade-Duncan parameter
a,b,c,d,n	fitting parameters

Figure 4.8. Elastoplastic model of Shao and Henry (1991), shown in the meridian plane and in the π-plane (Lade-Duncan surface).

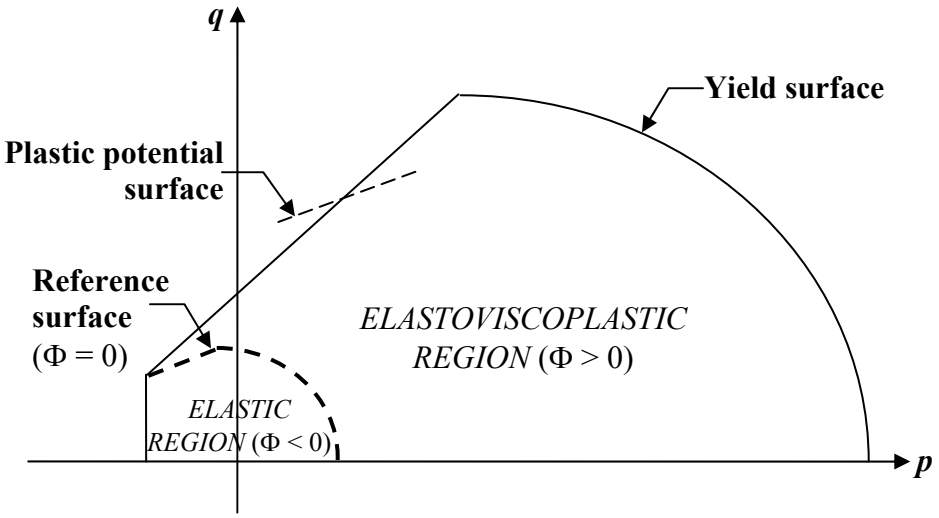

Figure 4.9. Overstress elastoviscoplasticity model of DeGennaro et al. (2003) and Datcheva et al. (2001), showing that reference surface has similar shape to yield surface or plastic potential surface.

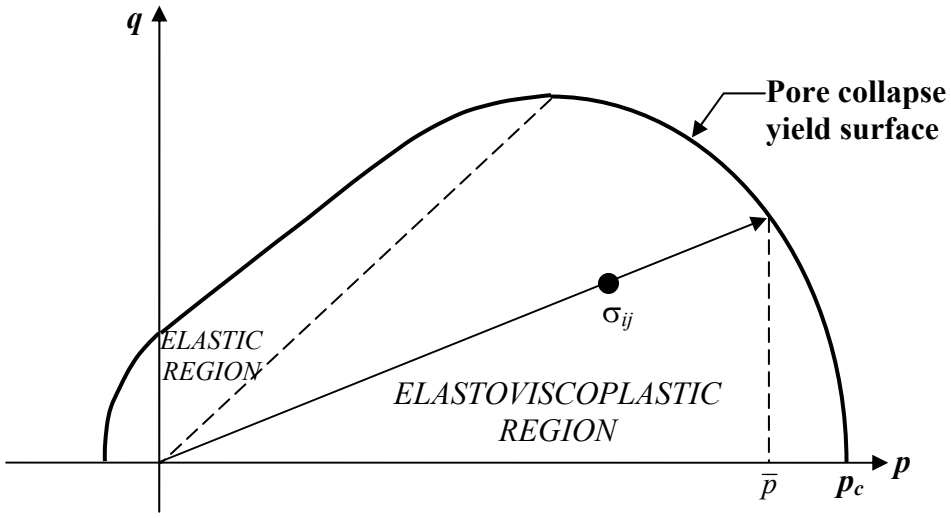

$$t_v = t_{vo}\left(\frac{\bar{p}}{p}\right)^{\frac{\lambda-\kappa}{\psi}}$$

$$\dot{\varepsilon}_v^{vp} = \frac{\psi}{1+e}\frac{1}{t_v}$$

$$\dot{\varepsilon}_{ij}^{vp} = \dot{\varepsilon}_v^{vp}\frac{\partial g/\partial \sigma_{ij}}{\partial g/\partial p}$$

$\bar{p}$	equivalent zero-age stress
λ	compression coefficient
κ	recompression coefficient
ψ	creep parameter
t_v	volumetric age
t_{vo}	minimum volumetric age

Figure 4.10. Rate-type elastoviscoplasticity model of Gutierrez (1999) shows that volumetric age and viscoplastic strain rate depend on distance between the stress point and the pore collapse yield surface.

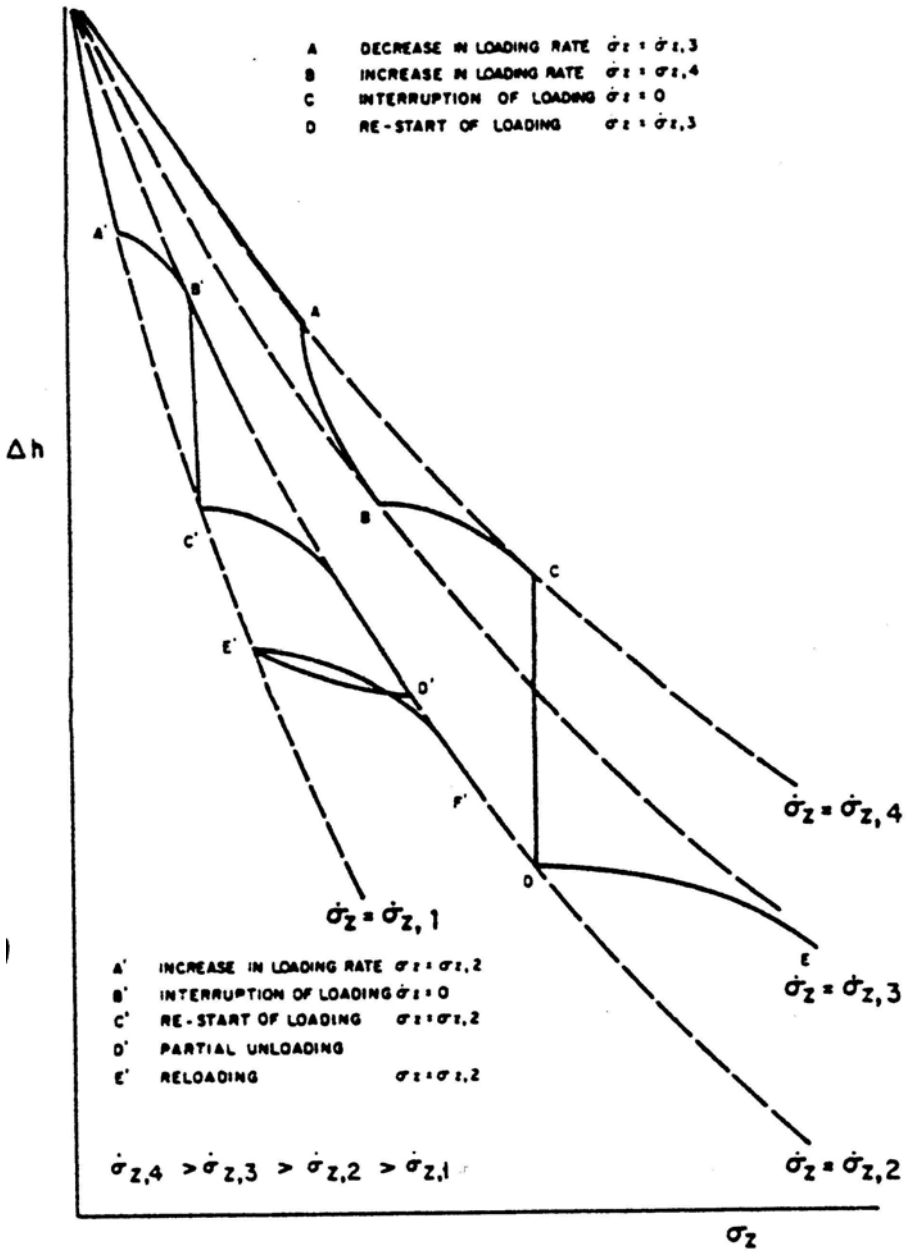

Figure 4.11. Rate-type elastoviscoplastic model of deWaal (1986) is similar to that of Bjerrum (1967), but is based on the principle of equal stress rates instead of time-lines and equivalent viscoplastic strain rates (deWaal and Smits, 1988). Compare to Figure 2.5.

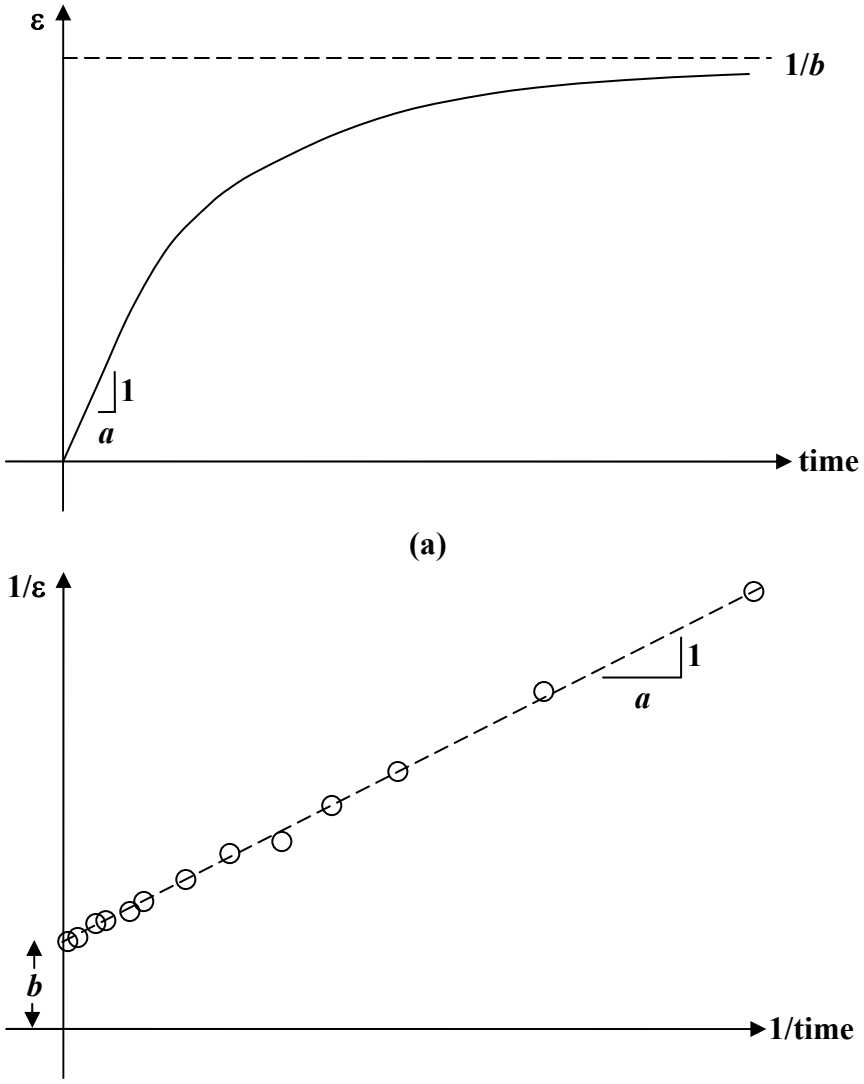

Figure 4.12. Hyperbolic time-dependent model is characterized by a limiting strain value shown in (a). Model parameters are found from creep test data by plotting (1/time) versus (1/creep strain) as shown in (b).

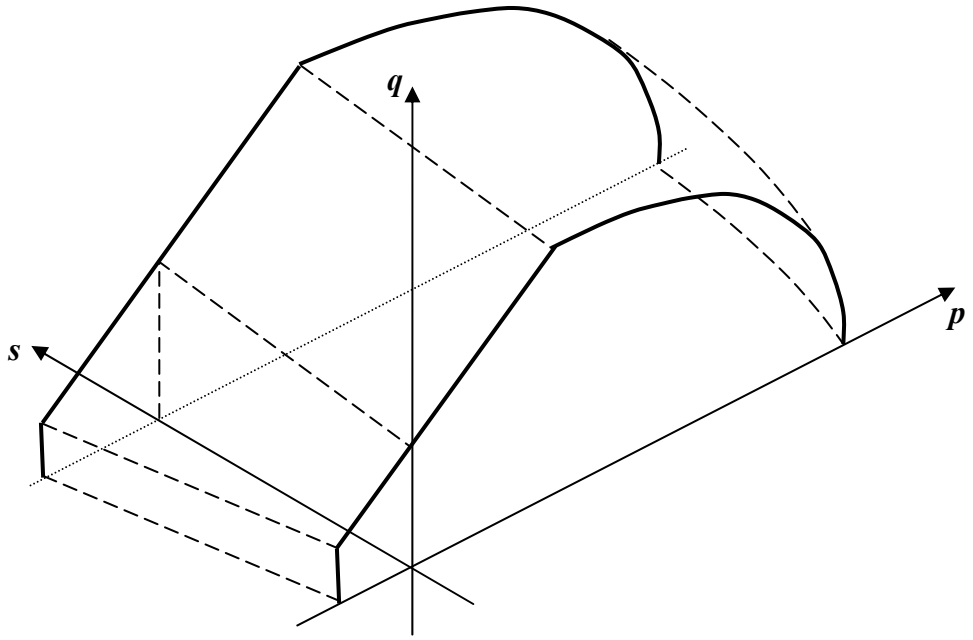

$$\dot{\varepsilon}_{ij} = \dot{\varepsilon}_{ij}^{m,e} + \dot{\varepsilon}_{ij}^{s,e} + \dot{\varepsilon}_{ij}^{m,p} + \dot{\varepsilon}_{ij}^{s.p}$$

$$\dot{\varepsilon}_{ij}^{m,e} = C_{ijkl}^{e}\dot{\sigma}_{kl}$$

$$\dot{\varepsilon}_{ij}^{s,e} = \frac{\kappa}{(1+e)}\frac{\dot{s}}{(s+p_a)}\delta_{ij}$$

$$\dot{\varepsilon}_{ij}^{m,p} = \dot{\lambda}\frac{\partial g}{\partial \sigma_{ij}}$$

$$\dot{\varepsilon}_{ij}^{s,p} = \frac{\lambda-\kappa}{(1+e)}\frac{\dot{s}}{(s+p_a)}\delta_{ij}$$

$$s = u_o - u_w$$

m	mechanical component
λ	compression coefficient
κ	recompression coefficient
s	suction or suction component
u_o	oil pressure
u_w	water pressure
p_a	atmospheric pressure

Figure 4.13. Components of the Barcelona Basic Model (Alonso et al., 1990) applied to chalk behavior in the models of DeGennaro et al. (2003) and Collin et al. (2002). All yield surfaces are enlarged under greater suction as shown in *p*-*q*-*s* space (after Collin et al., 2002).

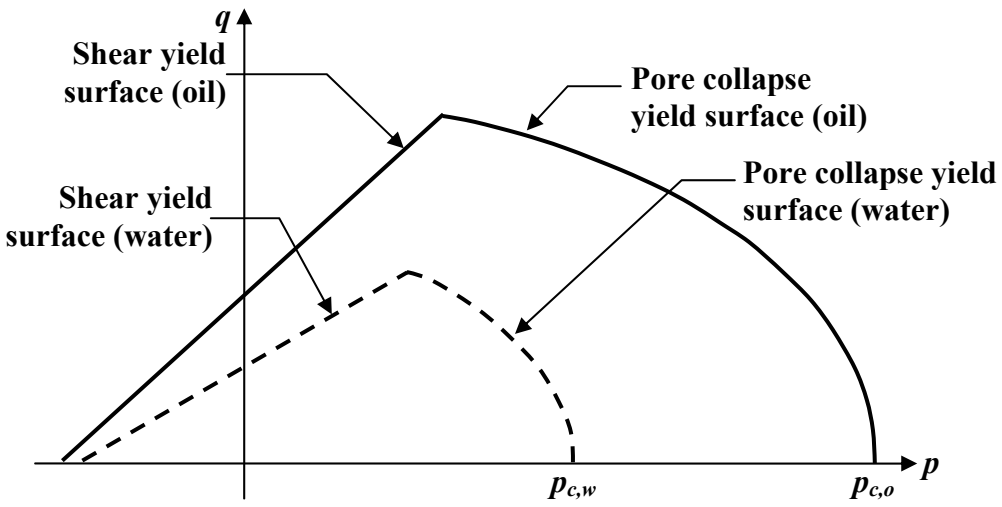

$$d\varepsilon_{ij} = d\varepsilon_{ij}^{e} + d\varepsilon_{ij}^{p} + \Delta\lambda_{w}\frac{\partial g}{\partial \sigma_{ij}}$$

$$\Delta\lambda_{w} > 0 \quad for\ S_{wi} < S_{wc} < S_{wf}$$

$$\Delta\lambda_{w} = 0 \quad for\ S_{wi} > S_{wc}\ or\ S_{wf} < S_{wc}$$

λ_w	water-induced plastic multiplier
S_{wi}	initial water saturation
S_{wf}	final water saturation
S_{wc}	critical water saturation

Figure 4.14. Pore fluid-dependent model of Homand and Shao (2000) differs from the Barcelona Basic Model because the yield surface changes abruptly when water saturation increases to the threshold value (after Homand and Shao, 2000).

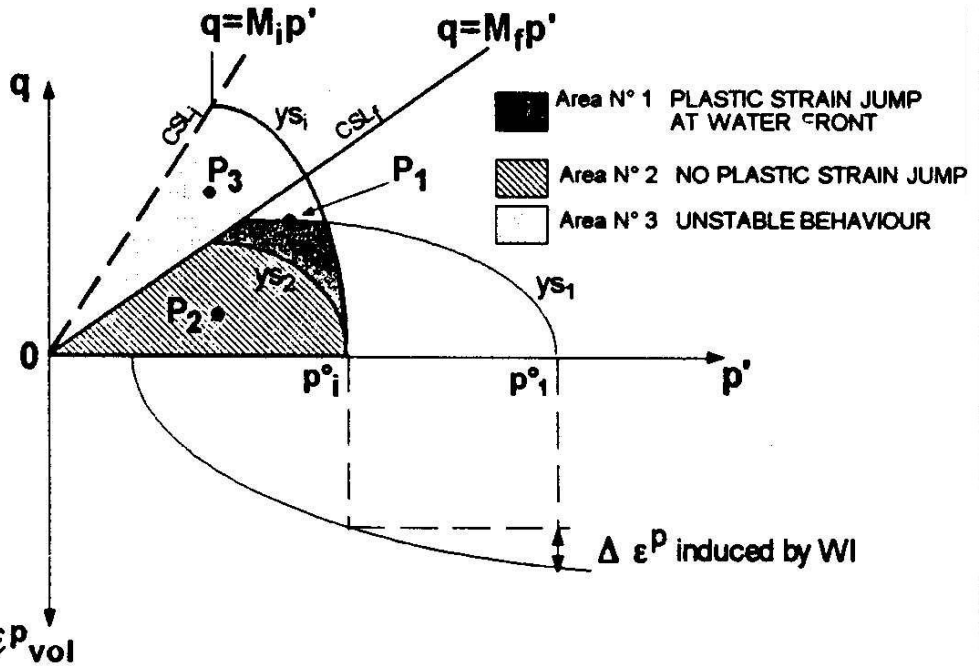

Figure 4.15. The pore fluid-dependent model of Piau and Maury changes the size of the yield surfaces as a function of water saturation, including changes in preconsolidation stress, friction angle, and critical shear stress ratio. Instantaneous change in yield surface produces a "yield surface jump at the waterfront" (Maury and Piau, 1996).